Multipactor Analysis of High-Power Ku-Band Orthomode Transducers (OMTs) in Aluminum Selective Laser Melting (SLM)

C Stoumpos, J-A Duran-Venegas, T Pierré, M García-Vigueras

Multipactor Analysis of High-Power Ku-Band Orthomode Transducers (OMTs) in Aluminum Selective Laser Melting (SLM)

C. Stoumpos[(1), (2)], J. A. Duran-Venegas[(2)], T. Pierré[(2)], M. García-Vigueras[(1)]

[(1)]*University of Rennes, CNRS, Institut d'Electronique et des Technologies du numéRique (IETR) — UMR CNRS 6164, F-35000 Rennes, France*
Charalampos.Stoumpos@insa-rennes.fr, Maria.Garcia-Vigueras@insa-rennes.fr

[(2)]*Thales Alenia Space, Antenna Product Line Department, 26 avenue Jean-François Champollion, B.P. 1187 31037 Toulouse Cédex 1, France*
juan-antonio.duran-venegas@thalesaleniaspace.com, thierry.pierre@thalesaleniaspace.com

INTRODUCTION

The multipactor is a very critical phenomenon and plays a determining role in the design and development of microwave components in satellite payloads [1]-[3]. The multipactor relates to a resonant RF electron discharge in which electron multiplication takes place due to the secondary electron re-emission process. The discharge is mainly encountered in RF accelerating structures where the combination of RF fields and clean surfaces of high secondary yield metals (e.g., copper or aluminium) will increase the number of electrons at each impact [4]. For the estimation of the multipactor and for sensing the maximum power that can be handled by a microwave component where a breakdown event can be avoided, we are mostly interested in the two following conditions: i) the synchronization of electron movement with the RF fields and ii) the electron multiplication via secondary electron emission. The latter is normally addressed relying on semi-empirical models of the Total Electron Emission Yield (TEEY) (Vaughan, Furman) or curves derived from measurement of an equivalent surface [5].
Additive manufacturing (AM) techniques employing metallic powder, such as Selective Laser Melting (SLM), offer important design freedom [6], lower mass and advantages for the implementation of devices supporting high power and potentially presenting lower TEEY. The main reason is the appearance of surface roughness [7] and fewer flanges which, in turn, reduce the likelihood of inter-modulation products. Still, AM imposes its own mechanical constraints that should be taken into account in order to allow to minimize the tolerances and the appearance of undesired supports.
In this paper, we present three topologies of Orthomode Transducers (OMTs) specially conceived to match the requirements of SLM in Aluminum for future satellite applications requiring high power handling. The orthomode transducers are of great importance for the RF chain of satellite payloads. They are physically 3-port microwave networks, while electrically are represented by a 4-port network where the common waveguide port excites, ideally, a set of two fundamental, orthogonally polarized and degenerate (same propagation constant/guided wavelength) modes [8]. In the case of a square waveguide, this set is the TE_{10} and TE_{01} modes, while in the case of a circular waveguide this set is the TE_{11h} and TE_{11v}, where the indices *h* and *v* stand for the horizontal and vertical polarization, respectively. An OMT is used to separate the two orthogonally polarized modes.
The benchmarking of this structure with similar ones in the literature that are manufactured with milling, allows to conclude that SLM devices perform better in terms of power handling. The multipaction is analyzed with CST PARTICLE STUDIO™ by Particle-In-Cell (PIC) simulations [9], [10]. The environment adopts the TEEY extracted by experimental data from measurements of a 3D-printed in SLM AlSi10Mg sample without any further surface post-treatment process, like for example surface finishing (i.e., polishing) or metallization (i.e., silver-plating).

3D-PRINTING ORIENTED ORTHOMODE TRANSDUCERS AND SIMULATION ENVIRONMENT

The three designed OMTs which were chosen as candidate solutions and are the subject of multipactor analysis are depicted in Figs. 1(a)-(c); we can see three different topologies also known as the Side-Branching, the Turnstile and the Bøifot junctions, respectively. All three OMTs have been designed so as to be realized by the additive manufacturing (or 3D-printing) technology in the framework of a joint project between Thales Alenia Space and IETR which relates to the research of this manufacturing technique so as to realize microwave components for satellite applications.
Figs. 2(a)-(c) show the schematic diagram representation of the three afore-mentioned OMT topologies. As previously mentioned, OMTs are physically 3-port networks, while electrically are represented by a 4-port network where the common waveguide port excites a set of two orthogonally polarized modes. Fig. 2(a) shows that the Side-Arm OMT presents two input accesses (ports 1 and 2) without any power division before the common cavity and eventually the common square port 3. On the contrary, Figs. 2(b) and (c) show that the Turnstile and the Bøifot junctions, respectively, present two input accesses (ports 1 and 2), but before the connection of each access to the common cavity, E-plane power dividers have been inserted as a natural choice steming from the OMTs architectures. This internal power division scheme plays a determining role to the multipactor suppresion.

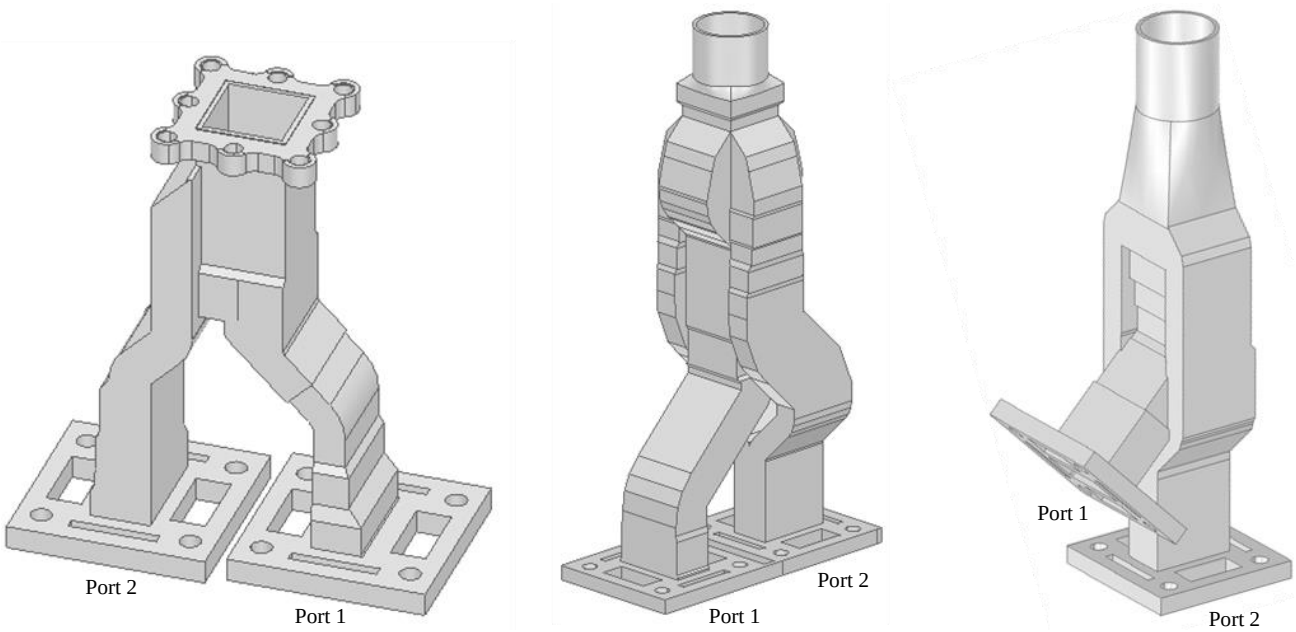

(a) (b) (c)

Fig. 1. Mechanical CAD models of the three invastigated Additive Manufactring oriented OMTs: (a) Side-Branching, (b) Turnstile and (c) Bøifot.

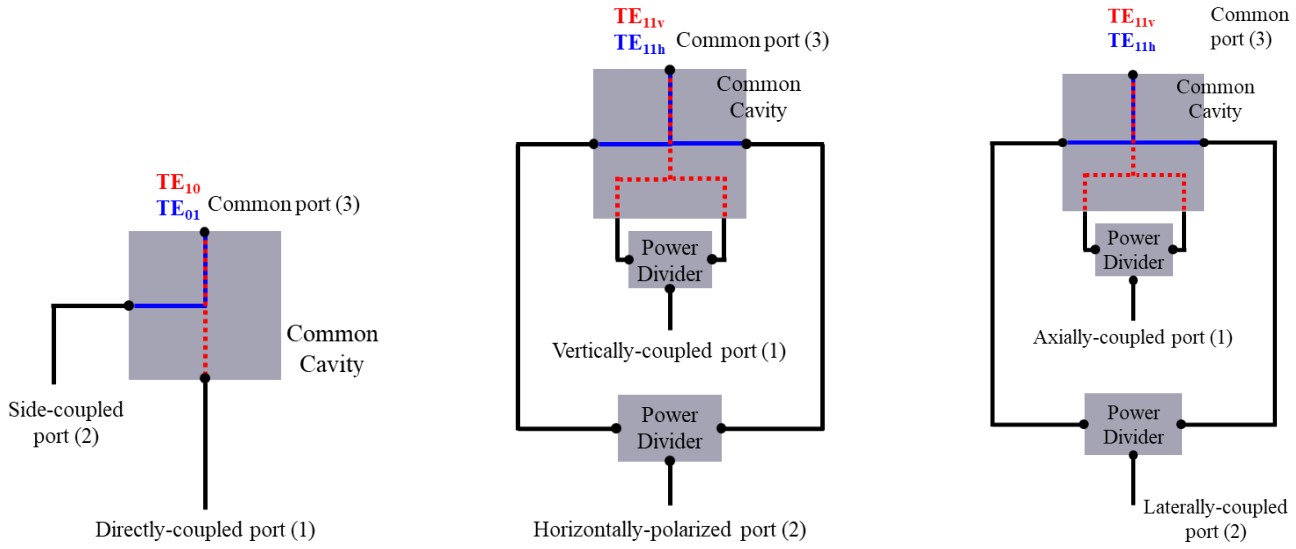

(a) (b) (c)

Fig. 2. Schematic diagram representations for the three invastigated Additive Manufactring oriented OMTs: (a) Side-Branching, (b) Turnstile and (c) Bøifot.

In this work, the multipaction is analysed with CST PARTICLE STUDIO™. The simulation environment adopts the Secondary Electron Yield (SEY) curve extracted by experimental data from measurements of a 3D-printed in Selective Laser Melting (SLM) AlSi10Mg sample without any further treatment of its surface. The curve of the SEY for surfaces in AlSi10Mg SLM is depicted in Fig. 3. The initial number of free electrons injected into each OMT is 10.000. Finally, we sweep the input power at the lowest, central and highest frequency. However, from prior knowledge as well as from simulations it is stated that the multipactor effect is more intense in the lower frequencies (therefore here we present the results only at 10.7 GHz as the worst case). Finally, we can extract the curve of the number of particles versus time for different levels of input power. From these curves we monitor the maximum power level that can be handled by each OMT without RF breakdown or in other words accumulation due to exponential growth of electrons travelling and bouncing onto the structure's metallic walls.

NUMERICAL RESULTS

This section presents the numerically calculated results of the multipactor analysis for the three OMTs under investigation from Fig. 1. It is first mentioned that the typical specification for high-power RF chain applications call for OMTs operation in multipactor-free mode for accepted power levels up to 3 kW[1] (namely around 64.8 dBm).
Fig. 4 illustrates the curves of the side-branching OMT's multipaction analysis for different levels of input power at 10.7 GHz and for the excitation of port 1 [Fig. 4(a)] and port 2 [Fig. 4(b)]. According to the simulation results, the maximum power level that can be handled from the OMT without experiencing breakdown events is up to 79 dBm, which corresponds to a level around 80 kW. Next, Fig. 5(a) depicts the particles accumulation when port 2 is excited for a multipactor-free case (P_{in} = 79 dBm and at 30 ns). Figs. 5(b) and 5(c) depict two cases where multipaction occurs for excitation of port 2 (P_{in} = 81 dBm at 80 ns) and port 1 (P_{in} = 79 dBm at 50 ns), respectively. As expected, and can be seen from the case of Fig. 5(b), the secondary electron emission is dominant near the lateral (side-branch) slot and multipaction occurs. Similarly, as we see from the case of Fig. 5(c), when port 1 is excited the secondary electron emission is dominant and multipaction occurs at the discontinuity of the first E-plane bend which exhibits the smallest waveguide geometry for this polarization path. As it will be shown after, contrary to the case of the turnstile and Bøifot OMTs, the side-branching OMT does not include a power divider along the routing of the two orthogonally polarized signals. This is a disadvantage in terms of power handling capability (and hence multipaction related issues), as where power division occurs, each microwave component is called to handle the half of the input power.

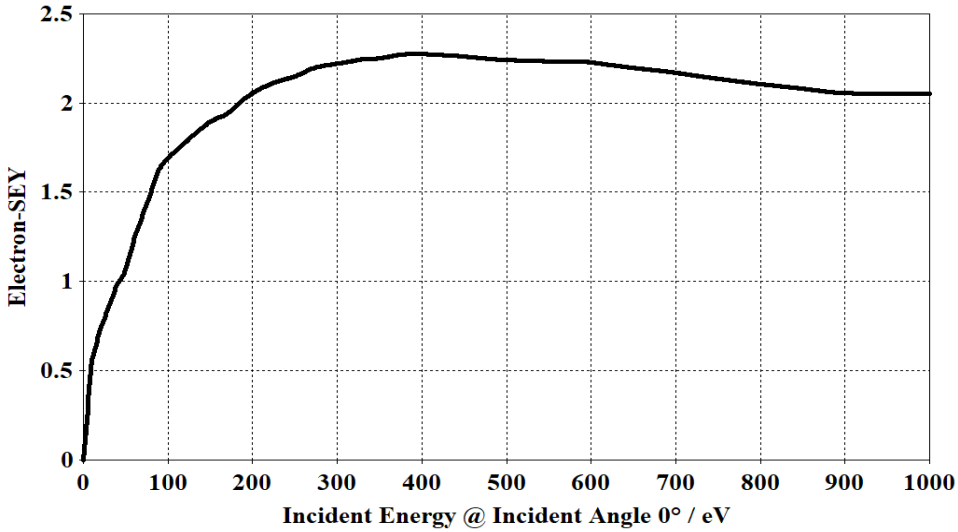

Fig. 3. Experimental Secondary Electron Yield (SEY) curve from measurements of an additively manufactured (in SLM) AlSi10Mg sample.

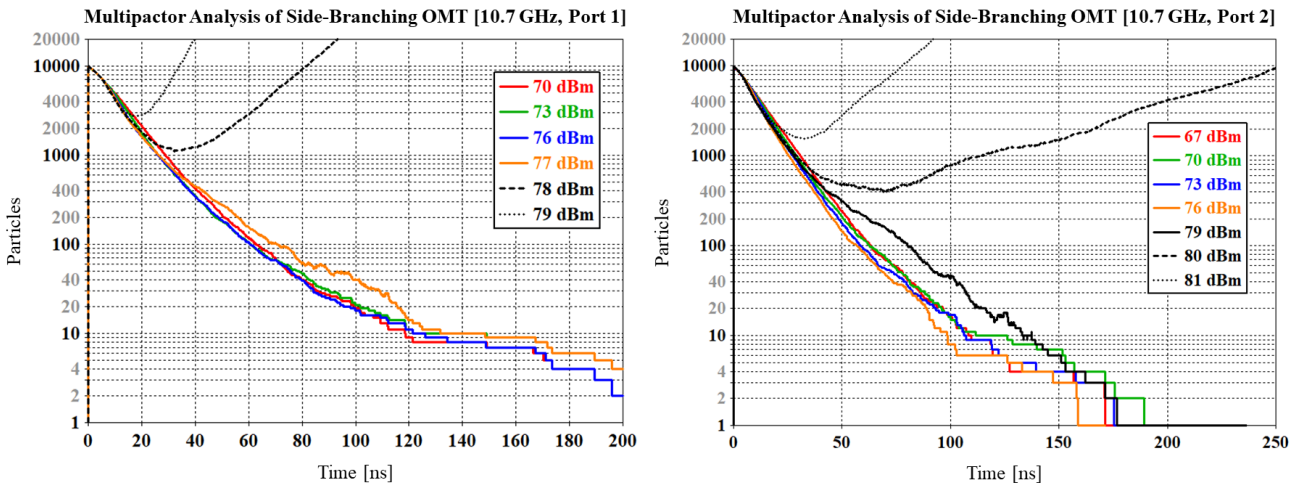

(a) (b)

Fig. 4. Multipaction analysis of the Side-Branching OMT [Fig. 1(a)] at the lowest operating frequency of 10.7 GHz: Number of particles versus time for different input powers and for excitation of: (a) port 1 and (b) port 2.

[1]ECSS Space Engineering Standard on Multipaction Design and Test, ECSS-E-ST-20-01C-DIR, June 2020, for a maximum nominal CW power per access as defined above. (CW → Continuous Wave)

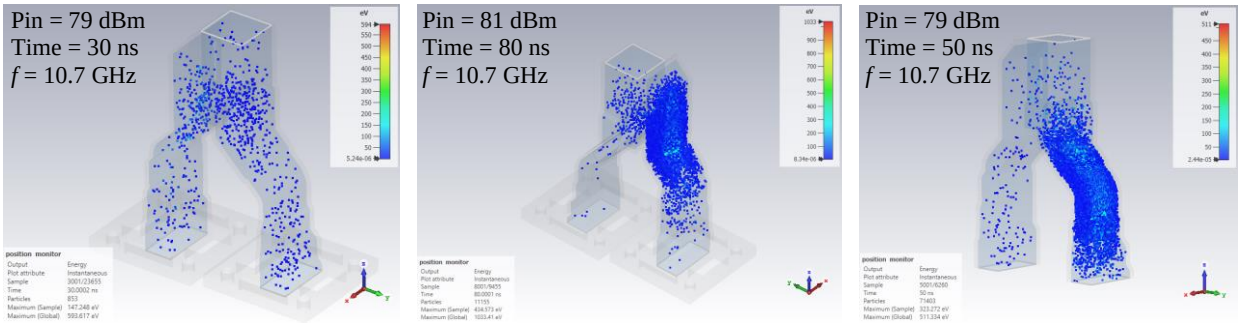

(a) (b) (c)

Fig. 5. Particles accumulation of the Side-Branching OMT [Fig. 1(a)] at 10.7 GHz in a: (a) multipactor-free case for excitation of port 2, P_{in} = 79 dBm and at 30 ns, (b) case where multipaction occurs for excitation of port 2, P_{in} = 81 dBm and at 80 ns and (c) case where multipaction occurs for excitation of port 1, P_{in} = 79 dBm and at 50 ns.

We proceed with the results linked to the multipaction analysis of the turnstile OMT [Fig. 1(b)]. Figs. 6(a) and 6(b) depict the number of injected particles and their progression versus time for different input power levels, at 10.7 GHz and for excitation of port 1 and port 2, respectively. The results show that the OMT does not multipact for input power levels of up to 83 dBm which corresponds to 200 kW. This upper limit of power that can be handled by the OMT occurs from port 2 and depends on the dimensions of the waveguides at the E-plane power divider's level. It is important to mention at this point that the turnstile OMT presents a great advantage in terms of power handling capability (and hence multipaction related issues). This is related to the fact that each orthogonally polarized signal routed in the OMT, is first split by an E-plane power divider to be later recombined at the common cavity. This means that a larger (at least double) amount of power can be handled by such OMT topologies in contrast to others (i.e., the side-branching or the double-ridge) that present one access per or even for one polarization path.

Next, we continue with the results of the multipaction analysis for the last OMT which is based on the Bøifot junction [Fig. 1(c)]. Figs. 7(a) and 7(b) illustrate the progression of injected particles versus time for different input power levels and for the excitation of port 1 and port 2, respectively. The results show that the OMT does not multipact for input power levels of up to 82 dBm which corresponds to about 160 kW. This upper limit of power that can be handled by the OMT occurs from port 2 and depends on the dimensions of the waveguide sections at the input of the E-plane power divider. It is mention that as in the case of the turnstile OMT, each orthogonally polarized signal routed in the Bøifot OMT is split by an E-plane power divider to be later recombined at the common cavity. This is a significant advantage in terms of multipaction as power division signifies that a larger amount of power can be handled.

Next, all AM-oriented OMT solutions proposed in this work are compared in Table 1. We can observe that for satellite applications which call for broad bandwidth (e.g., the total Ku-band: 10.7–14.8 GHz) and high power-handling requirements, the Turnstile as well as the Bøifot junctions can provide the best performance. In this point, we add that in the trade-off analysis for the selection of the optimal OMT solutions we first included also another category of orthomode junction; the Double-Ridge OMT [11]. Nevertheless, although this type of OMT exhibits broad bandwidth

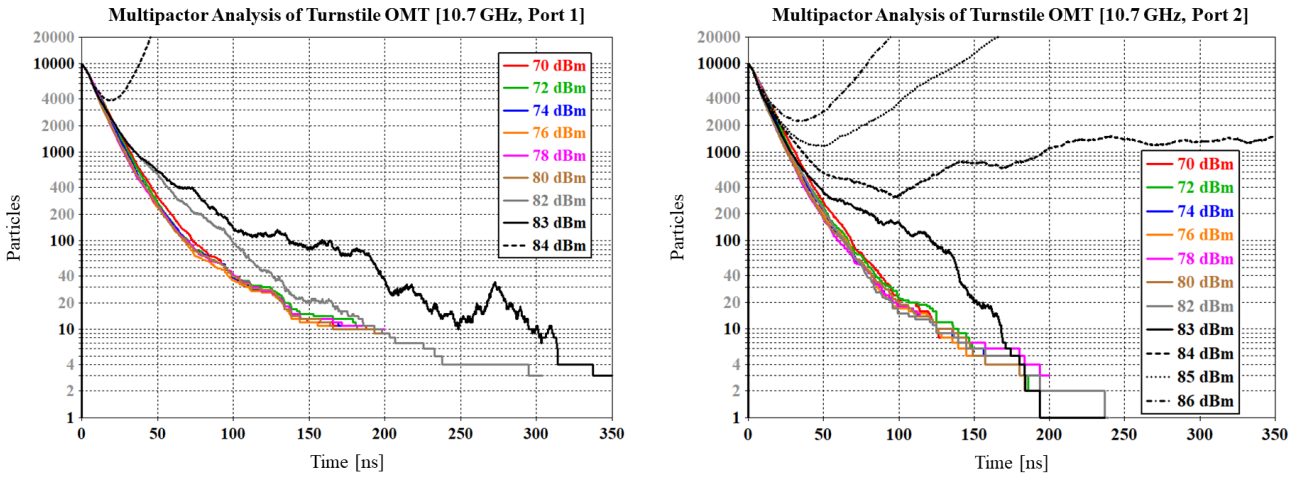

(a) (b)

Fig. 6. Multipaction analysis of the Turnstile OMT [Fig. 1(b)] at the lowest operating frequency of 10.7 GHz: Number of particles versus time for different input powers and for excitation of: (a) port 1 and (b) port 2.

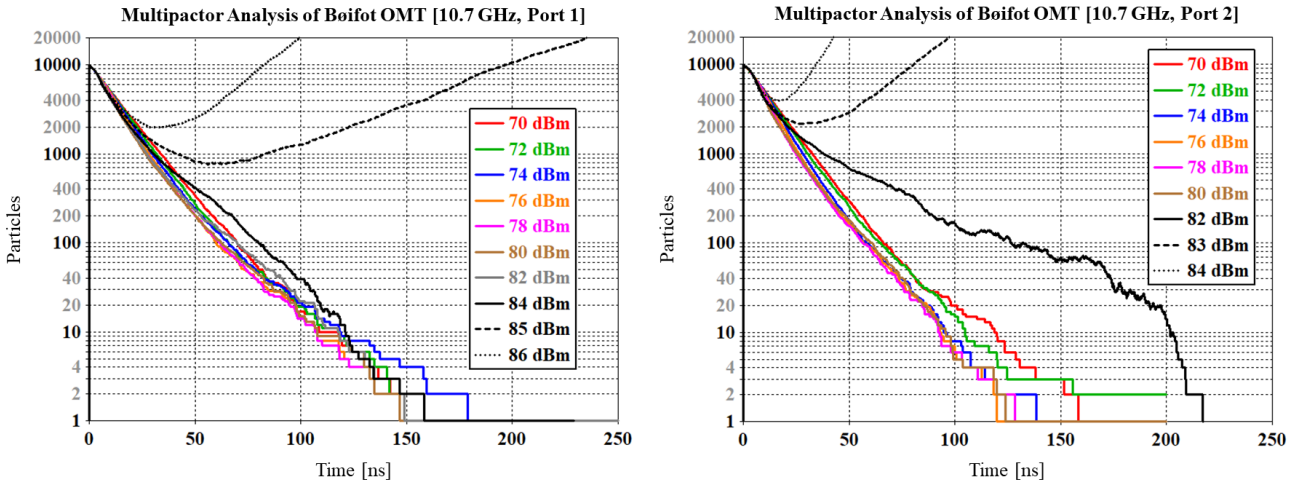

(a) (b)

Fig. 7. Multipaction analysis of the Bøifot OMT [Fig. 1(c)] at the lowest operating frequency of 10.7 GHz: Number of particles versus time for different input powers and for excitation of: (a) port 1 and (b) port 2.

Table 1. Comparison of the three proposed AM-oriented OMT solutions.

OMT→	**Side-Branching**	**Turnstile**	**Bøifot**
Operating Band	Ku-Tx (10.5-13 GHz)	Ku (10.5-15 GHz)	Ku (10.5-15 GHz)
Bandwidth	20%	35%	35%
Simulated Ohmic Losses	0.05~0.07 dB	0.06~0.11 dB	0.06~0.09 dB
Adaptability to 3D-Printing	Direct in z-axis (no inclination)	Direct in z-axis (no inclination)	Direct in z-axis (no inclination)
Multipaction (Max Power w/o Breakdown)	77 dBm (≈50 kW)	83 dBm (≈200 kW)	82 dBm (≈160 kW)

(similar to the Turnstile and Bøifot solutions), it also presents one single-access for the axially-polarized signal and hence its power handling capability is limited as no power division takes place. Thus, as expected, numerical results of a preliminary Double-Ridge OMT design showed maximum multipactor-free power levels similar to those of the Side-Branching OMT solution (i.e., around 80 dBm). The results and the analysis of the Double-Ridge OMT are omitted for sake of brevity. We highlight below three last and important points related to the subject of this paper:

i. Before the simulations with the experimental data from the SEY of Fig. 3 which relates to additively manufactured (in SLM) AlSi10Mg surfaces, we performed similar simulations with the Vaughan model's SEY from CST library which contains data related to tests performed on equivalent structures (samples) realized in milling. These tests were performed so that we can have a first idea on the multipactor of the three presented OMTs as well as to compare their performance. The simulation results with the SEY for milled surfaces (i.e., Vaughan model), qualitatively, showed the same trend with the results presented here (Figs. 4, 6 and 7). However, quantitatively, the values of the multipactor analysis showed a maximum power level that can be handled by all OMTs 4~6 dB lower compared to AlSi10Mg surfaces in SLM. In other words, the analysis with the SEY data from surfaces fabricated in (aluminium) traditional manufacturing presented a more conservative trend by 4~6 dB. This fact was expected and can be explained because, as known, 3D-printed structures exhibit additional surface roughness associated with the additive manufacturing technology compared to the traditional milling [6], [7]. Thus, as previously addressed in literature, additional roughness on a structure's surface enhances the immunity to multipaction [12]-[18]. Therefore, this difference between the two simulation environments (the two SEY which relate to traditional and additive manufacturing) verified the initial hypotheses for better performance in terms of multipactor for the 3D-printed (rougher) surfaces.

ii. For the final qualification of a microwave component in terms of multipactor, there are typically two principal manners the maximum power-handling level can be addressed. The first one is subjecting the device to high-power measurements and monitoring thereby its response, defining therefore experimentally the maximum power without breakdown. This method is apparently a safe way to characterize the multipactor of any microwave component, however, it requires lengthy, time-consuming and costly campaigns. The second way, includes the analysis presented above with simulations by numerical tools (i.e., CST Particle Studio) driven by data (SEY) from measurements of surfaces fabricated by the same manufacturing technology the final

microwave components will be built. However, when attempting to simulate the multipactor threshold, numerical calculations include inevitably some extent of uncertainty, which occurs mainly by the following factors:

a. Initial number of injected electrons
b. Frequency points
c. Differences between the simulated and manufactured models
d. Meshing and rest simulation uncertainties

Owing to the above-mentioned non-idealities introduced by numerical tools which lead to uncertainties with respect to the actual level of maximum power-handling, we are obliged to resort to pre-specified margins [19]; in our case, this margin is of the order of 7 dB. The calculation and definition of this margin is a task which includes detailed analyses as well as experimental high-power tests. It is therefore concluded that all OMTs can handle the required level dictated by the specifications (64.8 dBm) as well as the afore-mentioned margin.

iii. The last point to be added relates to the Passive Intermodulation (PIM) of the presented OMTs as well as in general of the 3D-printed microwave waveguide components. As known, when employing the AM technology, the structures are printed monolithically. This is a great advantage in terms of PIM, as in contrast to the milling technology, the structure of any microwave component does not need to be separated in different building blocks and assembled together with flanges and screws. This fact denotes that for 3D-printed components, the PIM risk is reduced.

Owing to its high power-handling level, excellent numerically calculated RF performance, low losses and compact profile, the OMT based on the Bøifot junction was fabricated in SLM using aluminium powder (AlSi10Mg). Fig. 8 depicts the 3D-printed OMT. No further treatment (e.g., polishing or metallization) of the OMT's surface was performed. Measurements of the OMT showed a good agreement with simulations and verified experimentally the robust numerically calculated RF performance of the device.

Fig. 8. Prototype of the 3D-printed Bøifot OMT in SLM using aluminium powder (AlSi10Mg).

CONCLUSIONS

In this work we present the multipactor analysis and results of three different OMT topologies tailored to 3D-printing. For the simulations, we use CST PARTICLE STUDIO™, where for the SEY, we adopted experimental data from measurements of a sample with additively manufactured (in SLM) AlSi10Mg surfaces. This study envisages to establish a criteria basis for the selection of optimal high-power OMT solutions in additive manufacturing. For this reason, three optimized CAD models of well-established OMT architectures have been compared to each other in terms of power handling capability. Although, all proposed solutions can meet the specifications (after also considering required margins due to numerical uncertainties), we demonstrated that OMTs which include power dividers in both channels to route the two orthogonally polarized signals can handle at least a double level of input power. After presenting the results for all OMTs, we last concluded to the fact that 3D-printed microwave components are more robust to high-power levels (more immune to multipaction) compared to components in milling as well as the performance of 3D-printed microwave components in terms of PIM is obviously superior owing to their monolithic body. In light of the favourable high-power and RF performance, on one hand, a general remark relates to the fact that the presented OMTs which comply with the additive manufacturing rules are competitive solutions with respect to the state-of-the-art. On the other hand, it is also highlighted that metal 3D-printing is not only an enabling fabrication technology for structurally complex microwave components which also present lower mass, but also a secure manufacturing option for the development of such components which exhibit power-handling levels significantly higher than equivalent ones in traditional manufacturing.

REFERENCES

[1] J. Vaughan, "Multipactor", *IEEE Trans. Electron Devices*, vol. 35, no. 7, pp. 1172-1180, Jul. 1998.

[2] F. Piro and Y. Brand, "PIM and multipactor considerations for future high-RF power space missions," *Proc. 8th Eur. Conf. Antennas Propag. (EuCAP'14)*, pp. 1643-1646, Apr. 2014.

[3] H. K. A. Nguyen, J. Mankowski, J. C. Dickens, A. A. Neuber and R. P. Joshi, "Calculations of Multipactor Growth in Rectangular Waveguides," *IEEE Trans. Plasma Sci.*, vol. 47, no. 2, pp. 1364-1371, Feb. 2019.

[4] N. Shafqat, F. Gerigk and R. Wegner, "Multipacting Simulations of Tuner-adjustable waveguide coupler (TaCo) with CST," e-Print: 1507.00444 [physics.acc-ph], Jul. 2015.

[5] J.R.M. Vaughan "Secondary Emission Formulas," *IEEE Trans. Electron Devices*, vol. 40, no. 4, p.830, Apr. 1993.

[6] O. A. Peverini *et al.*, "Selective laser melting manufacturing of microwave waveguide devices", *Proc. IEEE*, vol. 105, no. 4, pp. 620-631, Apr. 2017.

[7] R. G. Edwards, C. M. Norton, J. E. Campbell and D. Schurig, "Effective Conductivity of Additive-Manufactured Metals for Microwave Feed Components," *IEEE Access*, vol. 9, pp. 59979-59986, Apr. 2021.

[8] J. Uher, J. Bornemann, and U. Rosenberg, *Waveguide Components for Antenna Feed Systems: Theory and CAD*, Artech House, Boston, 1993.

[9] G. Burt, R. G. Carter, A. C. Dexter, B. D. S. Hall, P. Goudket and J. Smith, "Benchmarking simulations of multipactor in rectangular waveguides using CST-particle studio," *Proc. SRF*, vol. 9, pp. 321-325, Sep. 2009.

[10] M. C. Balk, "Simulation possibilities of vacuum electronic devices with CST PARTICLE STUDIO™," *Proc. IEEE Int. Vac. Electron. Conf.*, pp. 459-460, Apr. 2008.

[11] S. Asayama and M. Kamikura, "Development of double-ridged waveguide orthomode transducer for the 2 mm band," *J. Infr. Millim. Terahertz Waves*, vol. 30, no. 6, pp. 573–579, Jun. 2009.

[12] V. Nistor *et al.*, "Multipactor suppression by micro-structured gold/silver coatings for space applications", *Appl. Surf. Sci.*, vol. 315, pp. 445-453, Oct. 2014.

[13] W. Cui, R. Wang, T. Hu, J. Yang and Y. He, "Improvement multipactor discharge of microwave components by micro-porous surface," *Proc. 16th Int. Symp. Antenna Technol. Appl. Electromagn. (ANTEM)*, pp. 1-2, Jul. 2014.

[14] P. Martin-Iglesias *et al.*, "Enhanced multipactor performance in 3D printed microwave parts," *Proc. IEEE MTT-S Int. Microw. Workshop Series Adv. Mater. Process. (IMWS-AMP)*, pp. 1-3, Sep. 2017.

[15] D. Wu *et al.*, "Fabrication of porous Ag/TiO2/Au coatings with excellent multipactor suppression", *Sci. Rep.*, vol. 7, Mar. 2017.

[16] L. Olano, M. E. Dávila, J. R. Dennison, P. Martín-Iglesias and I. Montero, "Dynamic secondary electron emission in rough composite materials," *Sci. Rep.*, vol. 9, Sep. 2019.

[17] I. Montero *et al.*, "Low-secondary electron emission field under electron bombardment of microstructured surfaces, looking for multipactor effect suppression," *J. Electron Spectrosc. Relat. Phenom.*, vol. 241, May 2020.

[18] C. Stoumpos, M. García-Vigueras, J. -A. Duran-Venegas and T. Pierré, "Additively Manufactured High Power Microwave Components in Aluminum SLM," *Proc. IEEE ICOPS*, pp. 1-1, Sep. 2021.

[19] https://ecss.nl/standard/ecss-e-st-20-01c-multipactor-design-and-test-15-june-2020/